Image Segmentation using Local Probabilistic Atlases Coupled with Topological Information

Gaetan Galisot[1], Thierry Brouard[1], Jean-Yves Ramel[1] and Elodie Chaillou[2]
[1]*LI Tours, Université Francois Rabelais, 64 avenue Jean Portalis, 37000, Tours, France*
[2]*PRC, INRA, CNRS, IFCE, Université de Tours, 37380, Nouzilly, France*
{*gaetan.galisot, thierry.brouard, jean-yves.ramel*}*@univ-tours.fr, elodie.chaillou@tours.inra.fr*

Keywords: Atlas-based Segmentation, 3D Brain Images, Topological Information, Markov Random Field.

Abstract: Atlas-based segmentation is a widely used method for Magnetic Resonance Imaging (MRI) segmentation. It is also a very efficient method for the automatic segmentation of brain structures. In this paper, we propose a more adaptive and interactive atlas-based method. The proposed model allows to combine several local probabilistic atlases with a topological graph. Local atlases can provide more precise information about the structure's shape and the spatial relationships between each of these atlases are learned and stored inside a graph representation. In this way, local registrations need less computational time and image segmentation can be guided by the user in an incremental way. Pixel classification is achieved with the help of a hidden Markov random field that is able to integrate the *a priori* information with the intensities coming from different modalities. The proposed method was tested on the OASIS dataset, used in the MICCAI'12 challenge for multi-atlas labeling.

1 INTRODUCTION

In this paper, the segmentation of the subcortical brain structures in MRI is considered (as described in (Dolz et al., 2014)). We propose a new method based on a more local modeling of the different structures that need to be segmented and that increases the interactivity in order to be robust when some structures have an unexpected position or shape. This new modeling has first been designed for the case of 3D brain images, but it can be easily generalized for several others applications of image segmentation using *a priori* knowledge of shape and position of the regions.

In medical imaging, an atlas is a type of *a priori* spatial information which helps the localization of anatomical structures. The methods using this kind of atlases for the automatic segmentation of brain images have become very popular (Cabezas et al., 2011). However, these methods also suffer from several drawbacks. The segmentation of only one region needs the registration of the whole brain and can require an important computational time on 3D images with a high resolution. The second problem comes from the inter-individual variability; the atlas should be generic enough to describe effectively the whole population with a large anatomical variation but it should also be specific enough in order to give significant information about each region. One of the solution to obtain better segmentation results can be a selection of the information inside the different training images depending on the position in the brain image. For example, some multi-atlas methods use local information to improve the segmentation quality. (Shi et al., 2010; van Rikxoort et al., 2010). Note that the information provided by the user is rarely combined with this kind of atlas-based methods which are typically automatic. Another type of popular techniques is based on a graph representation of the brain to help and drive the segmentation. In (Colliot et al., 2006; Nempont et al., 2008; Al-Shaikhli et al., 2014), the authors use topological and spatial information to drive edges segmentation.

In this article, we proposed a new way to represent and use the *a priori* information during the segmentation. Brain structures are modeled by a graph in which the nodes represent the regions and the edges represent spatial relationships between regions. For each region, a specific probabilistic atlas is created and stored as attributes of the nodes. These atlases, composed of a probability map associated to a template image, are defined locally on a partial part of the image (not on the whole image such as the usual case). We call these atlases *local atlases*. Spatial relationships between each region of interest are extracted

Galisot G., Brouard T., Ramel J. and Chaillou E.
Image Segmentation using Local Probabilistic Atlases Coupled with Topological Information.
DOI: 10.5220/0006130605010508
In *Proceedings of the 12th International Joint Conference on Computer Vision, Imaging and Computer Graphics Theory and Applications (VISIGRAPP 2017)*, pages 501-508
ISBN: 978-989-758-225-7

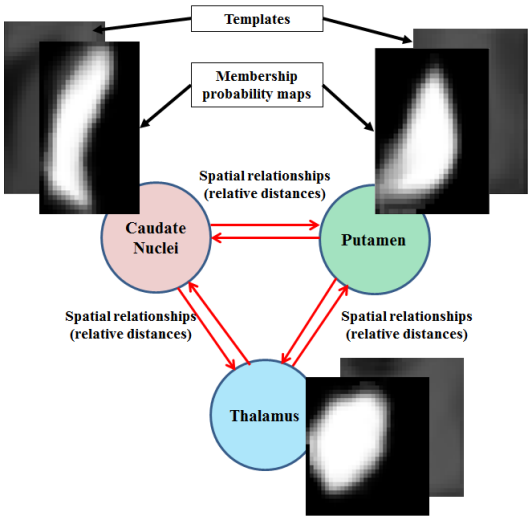

Figure 1: Schematic representation of *a priori* graph with 3 anatomical structures. Each node embeds a local atlas: a template and a membership probability map.

with the help of a training dataset and stored as attributes on the edges. The position and relative size of the regions (encoded in the edges) constitute the spatial relationships and are partially separated from the shape information encoded in the nodes of the graph. This *a priori* information is used during a sequential segmentation which is done through a Markov random field (MRF) classification.

2 CREATION OF THE TOPOLOGICAL GRAPH

The proposed method uses a graph in order to model and store the needed *a priori* information for segmentation. This graph is a complete one because spatial relationships exist between each region. Figure 1 shows an example of *a priori* graph that represents a structure containing three different regions.

2.1 Creation of Local Probabilistic Atlas

The atlas encodes the *a priori* knowledge about the shape of the region and the associated intensities in the different modalities. The local atlas is created in several steps (cf. Figure 2) starting from training data composed of N couples of MRI images and associated labeled images.

- Region delineation

The process of atlas creation is initialized by the delineation of the bounding box associated to each region represented in training dataset. Based on the N labeled available images and for each region r, the volume inside the bounding box of r and the volume associated in the MRI image are extracted and denoted L_r and B_r, respectively. A margin is added around each bounding box in order to better tolerate the possible variability (i.e, smoothing the edges inside the local atlas). This margin is a percentage of the real size of the bounding box. Throughout this paper, the bounding box will refer to this extended bounding box.

- Normalization

In order to correct the intensity of MRI images which can be different between one acquisitions and another, a normalization is performed for each region on the N images B_r. The method described in (Nyul et al., 2000) is applied in this case. This intensity normalization is local and achieved separately for each region r available in the training dataset.

- Reference image selection

A reference image is also needed for each region r. This reference has to be chosen from the images B_r. The image selected as a reference is the one minimizing the euclidean distance with all the other images inside the training set. The couple of reference images of the region r is denoted as L_r^0 and B_r^0. L_r^0 allows to compute the first iteration of the probability map of membership of voxels to r denoted by P_r^0 (if the voxel of L_r^0 is labeled *region*, the probability is fixed to 1, 0 otherwise). B_r^0 is the first iteration of local *template* of r. The template is denoted by T_r^0.

- Probability map and template construction

The template T and the probability map P are build incrementally. The transformations are done region by region and image by image considering all the available images in the training set. Considering the image whose number is I, a registration is performed from the image I to the current *template*. For that, the same process as before is followed, the volumes inside the bounding box of the region previously extracted (on the MRI and the labeled images) are denoted by as L_r^I and B_r^I, respectively. B_r^I is registered to the current *template* (T_r^0 for the first image) in two steps: a linear transformation (for a dimension adjustement) followed by a nonlinear registration is performed using Bsplines (Fornefett et al., 2001). The metric minimized by the transformation is the mean square error. This transformation is noted τ_2.

The template T and the probability map P are updated by averaging the current value with the registered information as follows:

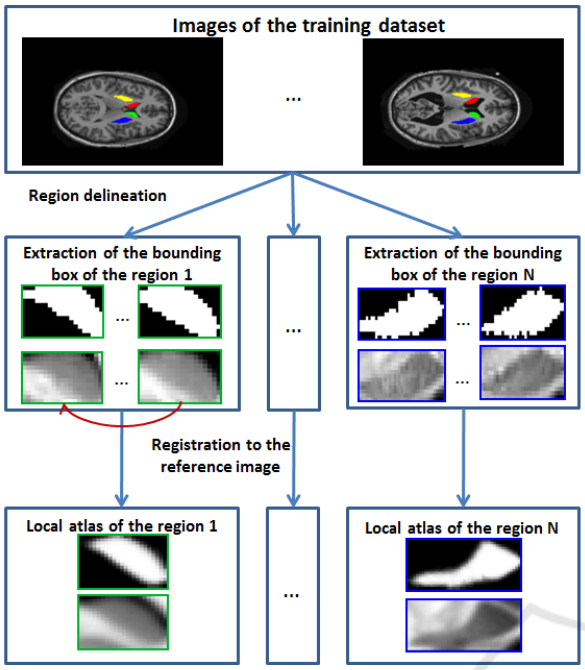

Figure 2: Outline of the local atlas construction.

$$\begin{cases} T_r^I = \frac{(T_r^{I-1} * I + \tau_2(\tau_1(B_r^I)))}{(I+1)}) \\ P_r^I = \frac{(P_r^{I-1} * I + \tau_2(\tau_1(L_r^I)))}{(I+1)}) \end{cases} \quad (1)$$

The registered region are parallelepipeds where the voxels intensities around the brain can be different from zero (unlike the complete brain image). A voxel V of the target image T_r^{I-1} can be linked to no voxel on the image to be registered B_r^I. In this case, the voxel V of the *template* keeps its value from the previous iteration and the voxel V of the probability map is updated considering the membership probability of the registered image as 0. For this kind of voxels V, $P_r^I[V]$ and $T_r^I[V]$ are updated as follows:

$$\begin{cases} P_r^I[V] = \frac{(P_r^{I-1}[V] * I)}{(I+1)}) \\ T_r^I[V] = T_r^{I-1}[V] \end{cases} \quad (2)$$

At the end of the process, each couple of images $\{T_r, P_r\}$ describes the local atlas of the considered region r and is stored inside the node of the graph corresponding to that region.

2.2 Creation of the Topological Relationships

The local atlas does not provide information about the position (of the bounding box) and the size (scale) of the region. In order to store this information, spatial relationships between each region are learned and incorporated into the edges of the so-called *topological graph*. It becomes then possible to deduce the position of a target region from the position of one or several source regions previously localized. Fuzzy spatial relationships have already been established in the past (Bloch et al., 2003) allowing to create a membership probability map compared to a reference structure. In our case, the problem is to automatically decide, as precise as possible, the position of the local atlas. The fuzzy membership information will be provided afterward by the local atlas.

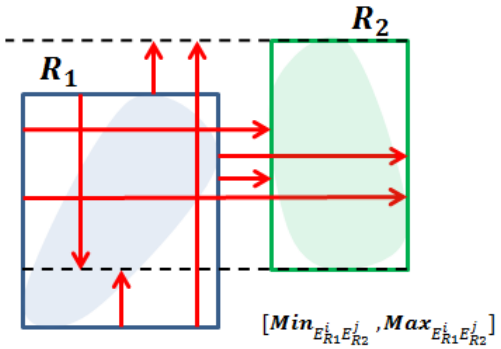

Figure 3: Distance relationships (8 relationships instead of 12 in 3D) from the structure R1 to the structure R2.

Twelve distances between the two structures to be linked have to be learned and stored in the graph in order to be able to deduce the position of a box from the position of another one (cf. Figure 3). The distance values are relative to the size of the source region, allowing to make the relation independent on the dimensions of the used images (and also the resolution of the image). For each of the 12 spatial relationships, the minimum and maximum relative distances, observed in the training set, are stored as an interval. The minimum and maximum relative distance between the side edge i of the region r_1 and the side edge j of the region r_2 are denoted by $Min_{E^i_{r1}E^j_{r2}}$ and $Max_{E^i_{r1}E^j_{r2}}$, respectively. In 3D, the side edges i and j can take 6 different values but the distance relationships Min and Max are defined only if i and j are in the same plane.

3 INCREMENTAL SEGMENTATION

3.1 Outline of the Segmentation

The segmentation (of a brain) uses all the information which is encoded inside the learned topological graph but in an incremental way. The desired regions have to be extracted one by one according to the decision

of an expert (i.e, a user) or by using a heuristic. The segmentation of a region is composed of several steps. First, the selection of the region to be segmented. Second, the positioning of its bounding box. Third, the registration of the local atlas inside the bounding box. Last but not least, the pixel classification with a MRF.

The position of the bounding box can be proceeded automatically or manually. In some cases, it can be interesting to let the user define or refine the position of the bounding box of a region in order to have an efficient segmentation inside it. The user can also let the algorithm use the spatial relationships learned previously (cf. Section 3.2) in order to automatically compute the position of the bounding box of the desired region; knowing that the user always has the possibility to correct the wrong positioning. When the bounding box is positioned, the box is inflated of several voxels in each direction in order to define the extended volume Be_R for the region R. This number of voxels is the same as during the atlas creation (10 % of the size of the bounding box). The margin decreases the impact of errors which could occur during the manual or automatic positioning.

From the nodes, the graph provides information about the region R: the probability map and the associated *template*. The *template* is registered to Be_R in the same way as during the atlas construction (cf. Section 2.1). The transformations τ_1 and τ_2 defining the registration is also applied to the probability map associated to the *template*. The result of this transformation initializes the process of voxel classification included inside Be_R giving a membership probability to the region for each voxel. The segmentation process, using a MRF, is described in Section 3.3.

3.2 Region Positioning

When at least one region has already been segmented, the spatial relationships stored in the edges of the graph can be used to determine the position of the new region to be segmented. All the regions already segmented are used as references to determine the position of the new bounding box. The set of regions already localized is denoted by R and the region we are looking for is denoted by r_{new}. The side-edges of the bounding box of r_{new} are positioned independently the ones with respect to the others. Six positions should be determined (two in each direction X, Y, Z defining the width, the height and the depth of the bounding box, respectively). The interval of minimum and maximum values $[min, max]$ are provided for each side edge by each region that is already positioned. Each region r include in R provides its information about the position of the region.

The first step is the transformation of the relative distances into real position in the image we want to segment. If we consider one direction on the image (X) and we search one of the two edges of r_{new}. The position of the edges of r, the size of the bounding box of r and the intervals of relative distance between r and r_{new}, provide two intervals of position denoted as $[Xmin_{E_r^1}, Xmax_{E_r^1}]$ (from the first edge of r) and $[Xmin_{E_r^2}, Xmax_{E_r^2}]$ (from the second edge of r).

We use the rectangular function $\Pi(x)$ with $x \in X$:

$$\Pi_r^1(x) = \begin{cases} 1 & \text{if } x \in [Xmin_{E_r^1}, Xmax_{E_r^1}] \\ 0 & \text{otherwise.} \end{cases} \quad (3)$$

In order to weight the different *a priori* information coming from each segmented region, a weight W is assigned to each interval ($[Xmin_{E_r^1}, Xmax_{E_r^1}]$) which is inversely proportional to its length. Thereby, the more precise the relation, the more it will have importance compared to the other intervals.

$$W_{E_r^1} = \frac{1}{Xmax_{E_r^1} - Xmin_{E_r^1} + \alpha} \quad (4)$$

where α is a parameter strictly positive, fixed to 0.1 in our case allowing to have a finite value for the weights.

All the intervals are combined together to obtain the final position of the edge of the region using the expected value of the sum of the intervals.

$$E_{rnew}^1 = Expected(\sum_{r \in R} W_{E_r^1} \Pi_r^1(x) + \sum_{r \in R} W_{E_r^2} \Pi_r^2(x)) \quad (5)$$

3.3 Voxel Classification

The hidden Markov random field is often used for image segmentation especially for the segmentation of MRI brain images. It provides satisfactory results not only for the segmentation of matters (Zhang et al., 2001) but also for the anatomical structures (brain nucleus) of the brain (Fischl et al., 2002). The HMRF performs the classification of the voxels in K distinct classes. The initialization is done with a *Kmeans* algorithm where the number of class K is fixed by the user. In the end, the voxels should be classified into two classes: *region* and *non-region*. However, the complexity of the tissues (in case of brain MRI images) cannot often be modeled by only 2 classes. Nevertheless, we make the hypothesis that the region we want to segment is composed of only one tissue and its intensity is homogeneous. One class is required to model the region intensity and 2 or 3 classes are needed to model the intensity outside the region. In practice, the results are similar if the number of

classes of the outside region is fixed to 2 or 3 independent of the region. At the end of the *Kmeans* algorithm, the class which has the highest number of voxels whose membership probability to the region R is important is labeled as *region*. All the other classes are referred to as *non-region*. The atlas information is provided by an external field. For the class defined as *region*, the external field is equal to -$log(atlas_i)$ and equal to -$log(1-atlas_i)$ for the other classes defined as *non-region*.

Then, the MRF has to classify the voxels inside the bounding box. The optimization problem is performed as in (Scherrer et al., 2009). The Expectation Maximization (EM) algorithm allows to optimize the Gaussian parameters that models the voxel intensities of each class. After the optimization, the voxels are classified into the most likely class. If the class's label is *non-region*, the voxel is not classified and could be classified during a future segmentation. If the class's label is *region*, the voxel is definitively assigned to the region R.

A parameter (α_i) supporting the atlas information and (β) supporting the neighborhood influence can modulate the energy function and were chosen empirically during experiments. So, the chosen values are $\beta = 0.05$ and $\alpha_i = 0.75 + 2 * H_i$ with H_i the entropy link to the *a posteriori* probability.

4 EXPERIMENTS

4.1 Dataset Description and Method Validation

The experiments were carried out on a dataset used in the Workshop MICCAI'12 (Landman et al., 2012) for the segmentation of cortical and subcortical regions with multi-atlas segmentation. This dataset is composed of T1 3D MRI images and of the associated ground truth (cortical and subcortical structures are available). Fifteen images are used to learn the *a priori* information and twenty images are used as test images where 13 subcortical regions have been chosen to test our method. The quality of the segmentation is evaluated by the Dice similarity coefficient defined as:

$$Dice = \frac{2*TruePositives}{2*TruePositives+FalsePositives+FalseNegatives}$$

The proposed method needs first the choice of the segmentation order given by the user in an interactively way and second the manual positioning of the first bounding box. In our study, the order of segmentation is fixed and same for all the segmentation.

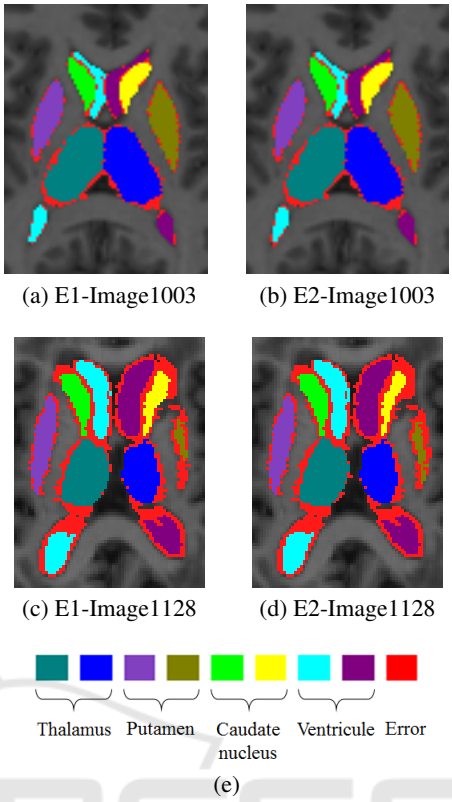

(a) E1-Image1003 (b) E2-Image1003

(c) E1-Image1128 (d) E2-Image1128

(e)

Figure 4: Results of a segmentation on an image close to images inside the training dataset, for the experiment E1 (a) and for the experiment E2 (b). Results of a segmentation on an image different from the images inside the training dataset, for the experiment E1 (c) and for the experiment E2 (d). The red pixels describe the pixels where the ground truth and the segmentation are not compatible.

The order was chosen arbitrarily while trying to select structures in both hemispheres. Two experiments were conducted:

- Experiment E1: the spatial relationships are not used and the bounding box are manually positioned with the ground truth for all the structures. In this experiment, the performance of the learning of the local atlas and MRF are evaluated.

- Experiment E2: The first 5 structures (*left caudate nuclei*, *right pallidum*, *left putamen*, *right thalamus*, *right ventricle*) are positioned perfectly according to the ground truth. The next structures are automatically positioned with the spatial relationships learned and stored in the graph.

4.1.1 Qualitative Results

The image (cf. Figure 4) demonstrates the results obtained on two brain images. The images (4a, 4b) represent the experiments E1 and E2 from a brain of a young person which is similar to the images inside

the training dataset of young people. The images (4c, 4d) represent the experiments E1 and E2 from a brain of an old person where the anatomical structures can be different from the structures inside the training dataset.

In both images, the experiments E2 give results with a similar quality than the experiments E1. The learned spatial relationships seem to be robust enough to not cause additional segmentation errors. The images (4c, 4d) shows some limits of the proposed method. Indeed, the differences between the training and test images are responsible of more errors; especially for the *ventricle* and *caudate nuclei* where the difference between old and young brains are important.

4.1.2 Quantitative Results

Table 1 describes the results obtained in experiments E1 and E2. Two methods used during the MICCAI'12 challenge are included. The method PICSL_BC explained in (Wang and Yushkevich, 2013) (the best one in the *multi-atlas labeling* challenge) and the CRL_STAPLE technique in (Avants et al., 2010).

When the structures are perfectly positioned with the ground truth information, the results of our method are similar to the state-of-the-art's method for the subcortical regions with an important size and relatively stable like the *putamens*, *thalamus*, *brain stem* and *pallidums* (around 2 or 3 lower than PICSL_BC). The detection of the *hippocampus* and *caudate nuclei* are a little bit under the state-of-the-art's results. However, they are close to the other methods. The quality of the segmentation of the ventricle is lower than the both methods described here. The lower results, shown in Table 1, can be explained by the utilization of probabilistic atlases. In contrary to multi-atlas, probabilistic atlas lose some information during the process of template creation.

When the brain structures (bounding boxes) are positioned in an automatic way, the obtained results are slightly lower than when the structures are positioned with the ground truth. The difference is around 3 points for most of the anatomical structures. Only the *caudate nuclei* is more different compared to the segmentation quality of experiment E1 (6 points). The margin of the bounding box is one of the reason explaining the results similar between E1 and E2.

Our method is coded in C++/Cli without any particular optimization. The computation time (on a PC, 2.70 Ghz and 16 Go Ram) is included between 20 seconds and 2 minutes 20 seconds for each region to be segmented, according to the size of the region and the parameters used for the registration. Furthermore, we can obtain suitable results (i.e, Dice coefficient average of experiment E1 is equal to 0.851 instead of 0.853), for the segmentation presented in the table, with a lower computation time (i.e, 22 seconds in average by region). Our method provides very fast results when we want to segment only some regions of the brain. This capability (computational time) is a strong advantage compared to the methods designed to deal with the whole segmentation of the brain. Such methods need around one hour of computational time as mentioned in (Wang and Yushkevich, 2013).

4.1.3 Segmentation of Sheep Brain Images

This work is part of a collaboration with the INRA (french national institute - http://www.inra.fr/). The goal is to create an adaptive segmentation tool that could be used on different types of brains (animal species). To demonstrate the flexibility of our method, the algorithm presented here has been applied on sheep brain 3D MRI images. Tests were performed on 3D T2 MRI images of sheep brains provided by the NeuroSpin platform [1]. These images were done on ex vivo brain in order to have better resolution (0.3 x 0.3 x 0.3 mm). Seven regions were labeled inside 4 images of the brain. Five regions are internal structures of the brain (*caudate nuclei*, *hippocampus* and *periaqueductal gray*), and 2 regions are cortical structures (*olfactory bulb*). A segmentation has been achieved on a fifth image in order to have a qualitative study.

In spite of the small number of images in the training dataset, an accurate segmentation can be obtained with the method when the bounding boxes are positioned manually (Figure 5). The segmentation of *caudate nuclei*, *hippocampus* and *periaqueductal gray* seem accurate. The *olfactory bulb* is more difficult to localize because of the variation between subjects in the cortical area. When we try to use the learned spatial relationships, the segmentation quality is more variable depending on the desired regions. In these first experiments, the *caudate nuclei* and *periaqueductal gray* needs to be manually positioned to obtain a correct segmentation. The *hippocampus* and *olfactory bulb* can be automatically localized depending on the previously segmented regions. The error in the positioning of the bounding boxes can be linked to the fact that brains are slightly deformed with ex vivo imaging, the distance relationships are then more variable. These results are promising for future works on animal brain images. The method could be tested on a higher number of brain structures and on different types of images like T1 in vivo images.

[1] NeuroSpin, CEA, Saclay, http://i2bm.cea.fr/drf/i2bm/Pages/NeuroSpin.aspx

Table 1: Similarity ratios of the segmentation of 13 subcortical regions on the MICCAI'12 dataset, for the methods E1, E2, PICSL_BC, CRL_STAPLE. The five first regions positioned with the ground truth are denoted by '*'.

Region	E1	E2	Method PICSL_BC	Method CRL_STAPLE
Caudate nuclei (left)	0.78 ∓ 0.25	0.78∓0.07 *	0.89 ∓0.07	0.84∓0.11
Caudate nuclei (right)	0.80 ∓ 0.06	0.74∓0.08	0.89∓ 0.07	0.82∓0.09
Pallidum (left)	0.83∓ 0.08	0.81∓0.19	0.87∓ 0.03	0.88∓0.02
Pallidum (right)	0.85∓ 0.07	0.85∓0.19 *	0.87∓ 0.05	0.88∓ 0.05
Thalamus (left)	0.87∓ 0.03	0.84∓0.04	0.91∓ 0.04	0.92∓0.03
Thalamus (right)	0.87∓ 0.03	0.87∓0.05 *	0.91∓ 0.05	0.91∓0.03
Putamen (left)	0.89∓ 0.05	0.89∓0.03 *	0.92∓ 0.01	0.91∓0.02
Putamen (right)	0.90∓ 0.04	0.88∓0.02	0.92∓ 0.01	0.91∓0.02
Ventricle (left)	0.81∓ 0.07	0.80∓0.09	0.93∓ 0.03	0.88∓0.05
Ventricle (right)	0.80∓ 0.07	0.80∓0.05 *	0.94∓ 0.03	0.87∓0.04
Hippocampus (left)	0.81∓ 0.03	0.78∓0.19	0.87 ∓ 0.02	0.84∓0.04
Hippocampus (right)	0.82∓ 0.03	0.82∓0.26	0.87∓ 0.02	0.84∓0.04
Brainstem	0.90∓ 0.01	0.89 ∓0.13	0.94∓ 0.01	0.93∓0.01

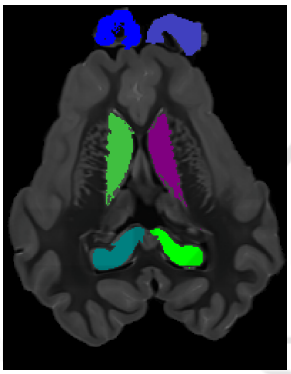

Figure 5: 2D image of a sheep brain with 6 regions segmented : *caudate nuclei, hippocampus* and *olfactory bulb*.

5 CONCLUSION

In this paper, we presented a method which can provide satisfactory results (compared to state-of-the-art methods designed specifically for the challenge) for the segmentation of several subcortical regions of the human brains. It is noticable that the proposed method can perform a fast partial segmentation as each region extraction is independent from the other. Furthermore, an expert user can decide the adequate order for the segmentation of the different structures we want to extract. The segmentation order can have an impact on the results. This method provides more precise information than usual atlas constructed with the same registration properties. Finally, thanks to the local characteristic of the *a priori* information, each local atlas can be learned separately. That is, the training set can be different for each region. Only the spatial relationships need some full images with several segmented regions inside. The flexibility of the proposed method has also been demonstrated by providing some qualitative results on sheep brains processed base on very few training samples. In our future work, several points in the method could be improved. First, the influence of the segmentation order or an incremental segmentation correction should be studied in order to limit the impact of the definitive segmentation. Second, the creation of the local atlases could be based on techniques less influenced by the selected reference image. Finally, it could be interesting to store more precise statistical information rather than only the minimum and maximum distances between the region borders.

ACKNOWLEDGEMENTS

This work has been partially supported by the NeuroGeo project funded by the Region Centre - Val de Loire. We would like to thank, Cyril Poupon for the acquisition of the ex vivo brain images perform in NeuroSpine and Ophélie Menant for the manual segmentation of the sheep brain images.

REFERENCES

Al-Shaikhli, S. D. S., Yang, M. Y., and Rosenhahn, B. (2014). Multi-region labeling and segmentation using a graph topology prior and atlas information in brain images. *Computerized Medical Imaging and Graphics*, 38(8):725–734.

Avants, B. B., Yushkevich, P., Pluta, J., Minkoff, D., Korczykowski, M., Detre, J., and Gee, J. C. (2010). The

optimal template effect in hippocampus studies of diseased populations. *NeuroImage*, 49(3):2457–2466.

Bloch, I., Géraud, T., and Maître, H. (2003). Representation and fusion of heterogeneous fuzzy information in the 3D space for model-based structural recognition - Application to 3D brain imaging. *Artificial Intelligence*, 148(1-2):141–175.

Cabezas, M., Oliver, A., Lladó, X., Freixenet, J., and Bach Cuadra, M. (2011). A review of atlas-based segmentation for magnetic resonance brain images. *Comput. Methods Prog. Biomed.*, 104(3):e158–e177.

Colliot, O., Camara, O., and Bloch, I. (2006). Integration of fuzzy spatial relations in deformable modelsApplication to brain MRI segmentation. *Pattern Recognition*, 39(8):1401–1414.

Dolz, J., Massoptier, L., and Vermandel, M. (2014). Segmentation algorithms of subcortical brain structures on MRI : a review. *Journal of Neuroimage*, page 200/212.

Fischl, B., Salat, D. H., Busa, E., Albert, M., Dieterich, M., Haselgrove, C., Van Der Kouwe, A., Killiany, R., Kennedy, D., Klaveness, S., Montillo, A., Makris, N., Rosen, B., and Dale, A. M. (2002). Whole brain segmentation: Automated labeling of neuroanatomical structures in the human brain. *Neuron*, 33(3):341–355.

Fornefett, M., Rohr, K., and Stiehl, H. (2001). Radial basis functions with compact support for elastic registration of medical images. *Image and Vision Computing*, 19(1-2):87–96.

Landman, B. A., Warfield, S. K., Hammers, A., Akhondi-asl, A., Asman, A. J., Ribbens, A., Lucas, B., Avants, B. B., Ledig, C., Ma, D., Rueckert, D., Vandermeulen, D., Maes, F., Holmes, H., Wang, H., Wang, J., Doshi, J., Kornegay, J., Hajnal, J. V., Gray, K., Collins, L., Cardoso, M. J., Lythgoe, M., Styner, M., Armand, M., Miller, M., Aljabar, P., Suetens, P., Yushkevich, P. A., Coupe, P., Wolz, R., and Heckemann, R. A. (2012). MICCAI 2012 Workshop on Multi-Atlas Labeling.

Nempont, O., Atif, J., Angelini, E., and Bloch, I. (2008). Structure Segmentation and Recognition in Images Guided by Structural Constraint Propagation. *European Conference on Artificial Intelligence ECAI*, pages 621–625.

Nyul, L. G., Udupa, J. K., and Zhang, X. (2000). New variants of a method of MRI scale standardization. *IEEE Transactions on Medical Imaging*, 19(2):143–150.

Scherrer, B., Forbes, F., Garbay, C., and Dojat, M. (2009). Distributed Local MRF Models for Tissue and Structure Brain Segmentation. *IEEE Transactions on Medical Imaging*, 28(8):1278–1295.

Shi, F., Yap, P.-T., Fan, Y., Gilmore, J. H., Lin, W., and Shen, D. (2010). Construction of multi-region-multi-reference atlases for neonatal brain MRI segmentation. *NeuroImage*, 51(2):684–93.

van Rikxoort, E. M., Isgum, I., Arzhaeva, Y., Staring, M., Klein, S., Viergever, M. a., Pluim, J. P. W., and van Ginneken, B. (2010). Adaptive local multi-atlas segmentation: application to the heart and the caudate nucleus. *Medical image analysis*, 14(1):39–49.

Wang, H. and Yushkevich, P. A. (2013). Groupwise segmentation with multi-atlas joint label fusion. *Lecture Notes in Computer Science (including subseries Lecture Notes in Artificial Intelligence and Lecture Notes in Bioinformatics)*, 8149 LNCS(PART 1):711–718.

Zhang, Y., Brady, M., and Smith, S. (2001). Segmentation of brain MR images through a hidden Markov random field model and the expectation-maximization algorithm. *IEEE Trans Med Imag*, 20(1):45–57.